

Novel Design of Amine and Metal Hydroxide Functional Group Modified Onto Sludge Biochar for Arsenic Removal

Chih-Kuei Chen (✉ ckchen@niu.edu.tw)

National I-Lan University <https://orcid.org/0000-0002-3443-4275>

Nhat-Thien Nguyen

National Taipei University of Technology

Thuy-Trang Le

Duy Tan University

Cong-Chinh Duong

Southern Institute of Water Resources Research

Cong-Nguyen Nguyen

Dalat University

Duc-Toan Truong

Dalat Nuclear Research Institute

Research

Keywords: Fe-SB-DETA, sludge biochar, arsenic, density functional theory

Posted Date: August 9th, 2021

DOI: <https://doi.org/10.21203/rs.3.rs-764363/v1>

License: © ⓘ This work is licensed under a Creative Commons Attribution 4.0 International License.

[Read Full License](#)

Version of Record: A version of this preprint was published at Water Science and Technology on February 8th, 2022. See the published version at <https://doi.org/10.2166/wst.2022.047>.

Abstract

Among the arsenic removal technologies, the adsorption method is found to be an efficient, inexpensive and simple method with obvious advantages and application value for arsenic removal in water. While, each method has its limitations, the traditional adsorption method used for arsenic removal due to its high operating cost and low adsorption efficiency. Consequently, this study explicitly designed sludge biochar (SB) adsorbed for arsenic removal with lower operation costs and higher adsorption efficiency properties. Generally, biochar only relies on micropores for pollutant adsorption, but physical adsorption is not highly efficient for arsenic removal. Therefore, in order to improve the removal efficiency of arsenic by SB, diethylenetriamine (DETA) and FeCl_3 were used in this study to modify the surface of SB by an immersion method. The modified SB has not only pore adsorption characteristics but also electrostatic adsorption, oxidation-reduction and complexation characteristics. The objectives of this research are to obtain optimum operation conditions by assessing the effect of different Fe content, pH and initial concentration on adsorbing arsenic. The arsenic adsorption mechanism on SB was studied using Density Functional Theory (DFT) to understand the functional effect on arsenic adsorption. Results showed the presence of amine and iron oxyhydroxides functional greatly promoted SB surface activity and its arsenic adsorption potential. DFT model result is the same as the result of arsenic adsorption performance with the high adsorption energy. The reaction mechanism is divided into four pathways, including oxidation-reduction, complexation, electrostatic adsorption and pore adsorption.

1. Introduction

Arsenic is a concern in groundwater or wastewater treatment because of its health effects. Arsenic was classified as a substance that causes serious eye damage (Level 1), cancerogen (Level 1), skin irritating substance (Level 2), reproductive toxic substances (Level 2) and hazardous substances in water environment (Level 2). Arsenic is primarily used in solutions such as As(V) (H_2AsO_4^- , HAsO_4^{2-} and AsO_4^{3-}) and As(III) (H_2AsO_3^- , HAsO_3^{2-} and AsO_3^{3-}) [1]. In general, As(III) is more toxic than As(V) because the former binds to single but more closely related groups of nearby sulfhydryls that react with a variety of proteins and inhibit their activity. Owing to electronic configuration As(III) is more stable than As(V) [2–3]. The presence of arsenic in water is attributed to natural weathering processes, geochemical reactions, biological activity, combustion of fossil fuels, volcanic eruptions, gold mining, leaching of man-made arsenic compounds, metal ores smelting, desiccants, wood preservatives and agricultural pesticides, and many other anthropogenic activities [3]. Arsenic is toxic and induces hyper-pigmentation, muscle weakness, skin thickening, neurological disorders and human cancer. The main route of human exposure is drinking arsenic contaminated groundwater. Hence, the arsenic level for drinking water has been reduced by the World Health Organization to $10 \mu\text{g L}^{-1}$ [4].

The approaches for arsenic removal from water sources include chemical precipitation, membrane processes, reverse osmosis, oxidation, ion exchange [5, 6] and electro coagulation treatment [7]. Recent research focused on the use of possible adsorbents, many adsorbents were used for arsenic adsorption

based on agriculture and industrial waste, surfactants, carbon-based materials, polymers and metal oxides [8, 9]. Especially, metal oxides such as iron-doped amino-functionalized sawdust [10], isolated ferric ion combined on chelate resin [11], magnetic gelatin modified biochar [12], iron hydroxide/manganese dioxide [13], activated carbon–alumina composites [14], nano zero-valent iron [15, 16], TiO_2 [17], CeO_2 [18], CuO [19], Fe_2O_3 [20, 21], Fe_3O_4 [22], CaO [23], ZrO_2 [24] and GNPs/ CuFe_2O_4 [25] have been extensively studied in aqueous solution for arsenic treatment due to their high affinity with arsenic species, low cost and adsorption capability tunability.

An alternative carbon source is readily available in the form of urban sludge, which is currently managed as a waste in Taiwan. The quantity of waste sludge has been steadily increasing in the country, thus requiring the government to spend a large amount of money for the management of this waste. Therefore, it is important to develop one step facile and quick preparing method for high efficiency for arsenic removal. Sludge Biochar (SB) has been identified as an effective adsorbent that can be used to remove various heavy metals dissolved in water, because the specific surface area and micro-porous structures of SB are high. While, SB hosts several surface functional groups, such as carboxyl ($-\text{COOH}$) and hydroxyl ($-\text{OH}$), for adsorbing heavy metal effectively. These groups can work through electron donation, cation exchange, electrostatic attraction, or surface complexation to effectively remove arsenic. In other hand, to understand the effect of amine and iron oxyhydroxides functional groups on the SB's surface to adsorb arsenic, diethylenetriamine (DETA) and iron metals were used to modify the SB and improve the effects of adsorption arsenic. In this particular adsorption, the particles of iron oxyhydroxides found on the SB surface are capable of replacing the As molecules OH- ligand, forming mono or bi-dentate complexes that enable them to be attached to the surface. This coordination occurs only in charged molecules previously attracted to the metal-SB surface, or in those molecules with sufficient energy to overcome the electrostatic repulsion with the metal-biochar surface. Thus, electrostatic repulsion between negative surface charge of metal-SB surface and As anions occurs. If these ionic molecules have difficulties in overcoming these electrostatic forces they cannot interact to a higher extent with metal particles and hence adsorption occurs to a lesser extent. Moreover, acidic properties bind efficiently As molecules allowing electrostatic interactions with metal oxyhydroxide particles and with acidic surface groups [26].

Additionally, the mechanism for the adsorption of arsenic on the SB surface is not yet clear. According to the previous study, a theoretical analysis of the mechanism of arsenic adsorption on the surface of SB prepared from urban sludge is hardly available. Therefore, the adsorption mechanism and the impact mechanism of metal oxides complexes on arsenic adsorption over the SB surface of urban sludge are very important [27]. The Density Functional Theory (DFT) has proven to be a successful research tool for adsorption and reaction theoretical analysis. Mechanism for adsorption of arsenic on SB and composites of metal oxides is systematically investigated by DFT calculation in this research. The objectives of this work are (a) to prepare SB and iron oxides composites, such as SB and Fe-SB-DETA for developing key reaction between arsenic and modified material; (b) to obtain optimum operation conditions by assessing the effect of different Fe content loading mass on adsorbing arsenic; (c) to obtain optimum operation

conditions by assessing the effect of pH and initial concentration on adsorbing arsenic; (d) to systematically calculate adsorption energy, bond distance and adsorbed structure through DFT; (e) to developing arsenic adsorption mechanisms.

2. Materials And Methods

2.1. Preparation of SB

To obtain the activated SB, this study used ZnCl_2 as the activator because ZnCl_2 requires a low activation temperature and the best pore-forming effect. First, different amounts of x% ZnCl_2 (x = 33, 50, 60 and 67%) were dissolved in 150 mL of distilled water. Then, 10 g of urban sludge was mixed with the ZnCl_2 solution and stirred at approximately $85 \pm 5^\circ\text{C}$ for 2 hr. The mixtures were dehydrated in an oven at $110 \pm 5^\circ\text{C}$ for about 24 hr. The ZnCl_2 impregnated urban sludge was placed in a ceramic crucible and pyrolyzed in a horizontal tubular furnace under nitrogen flow. The samples were heated to final temperatures of $450 \pm 5^\circ\text{C}$ with heating rate of $10^\circ\text{C min}^{-1}$ for residence time of 1 hr. The resultant SB was washed with 3 M HCl solution by heating at around $90 \pm 5^\circ\text{C}$ for 30 min to remove residual ZnCl_2 . In addition, it was filtered and rinsed by warm distilled water until neutral pH, dried at $100 \pm 5^\circ\text{C}$ in an oven for about 12 hr and weighed to calculate the yield.

2.2. Preparation of Fe-SB-DETA

Fe-SB-DETA was prepared following the method as described above. To obtain the activated material, the appropriate amount of DETA and different amounts of FeCl_3 (including 2.0, 4.0, 8.0, 16.0 and 32.0%) were dissolved in 150 mL of distilled water. Then, 10 g of the SB was mixed with mixture solution, and stirred at $85 \pm 5^\circ\text{C}$ for 2 hr. Then, the mixtures were dehydrated in an oven at $110 \pm 5^\circ\text{C}$ for 24 hr after filtered and rinsed by distilled water. Different composite materials are abbreviation as 2%Fe-SB-DETA, 4%Fe-SB-DETA, 8%Fe-SB-DETA, 16%Fe-SB-DETA and 32%Fe-SB-DETA.

2.3. Materials characterization

The specific surface area, pore size distribution and pore volume were determined by performing nitrogen adsorption-desorption measurements with an ASAP 2020 apparatus by using Brunauer-Emmett-Teller (BET) calculation methods. The crystal phase of the biochar was determined by an X-ray Diffraction (XRD) with employing Cu K α radiation wavelength of 0.15405 nm, accelerating voltage of 40 kV and current of 30 mA over the 2θ range of $20-80^\circ$. The Fourier Transform Infrared (FTIR) of the biochar was recorded to study the functional groups at room temperature. The metal valence on the surface of biochar was further determined by X-ray photoelectron spectroscopy (XPS). The interaction oxidation and reduction mechanism of metal ions on biochar was used Electrochemical Techniques (ECT).

2.4. Adsorption performance assessment

Adsorption isotherm experiments were carried out in 100 mL adsorption system. The sludge biochar were mixed with 50 mL of the appropriate arsenic solution at 25°C for 60 min. The solution was filtered with using a membrane filter (pore size 0.45 μm). In addition, an inductively coupled plasma atomic emission spectroscopy with a detection limit for arsenic of 10 ppb was used to evaluate the residual arsenic in the aqueous solutions. The test data were regularly calibrated using standard solution in order to obtain accurate data.

The exact amount of adsorbed As per adsorbent unit mass was determined by weight balance as follows Eq. (1):

$$q_e = \frac{C_o - C_e}{W} \times V1$$

Where, the equilibrium adsorption capacity is q_e (mg g⁻¹), V (mL) is the volume of As solution, W (mg) is the amount of adsorbent used in the experiments, C_o (mg L⁻¹) is the initial concentration of As and the balance concentration measured after adsorption stands for C_e (mg L⁻¹).

2.5. DFT model and computation detail

The SB surface is doped with amine functional group and iron hydroxide group to form other Fe-SB-DETA structures. The arsenic is adsorbed on the above Fe-SB-DETA structures respectively after 10 ns molecular dynamics simulation. Finally, adsorption systems were constructed in the same cubic simulation lattice built with their dimensions of $x = 10 \text{ \AA}$, $y = 10 \text{ \AA}$, and $z = 14 \text{ \AA}$.

In Materials Studio 2018, all the DFT calculations in this analysis were carried out using the DMol³ software kit [28]. The terms of exchange and correlation were determined in the form proposed by Perdew, Burke, and Ernzerhof using the Generalized Gradient Approximation [29]. The core DFT semi-core pseudo potential method was utilized to calculate the core treatment of DETA, for other elements, the all-electron method was applied [30]. Solvation effects were incorporated by conductor-like polarizable continuum model for all the systems with water as solvent. The adsorption energy (E_{ads}) of pollutant molecules on Fe-SB-DETA surface was calculated by the following Eq. (2) [31]:

$$E_{ads} = E_{Fe-SB-DETA-pollutant} - (E_{Fe-SB-DETA} + E_{pollutant}) \quad (2)$$

Where, $E_{Fe-SB-DETA}$ and $E_{pollutant}$ respectively represent the energies of the Fe-SBC-DETA surface and the single pollutant molecule, and the $E_{Fe-SB-DETA-pollutant}$ is the total energy of pollutant-Fe-SB-DETA complex. According to Eq. (2), a negative value of E_{ads} indicates that the process is an exothermic reaction and high negative value corresponds to a stronger interaction, which indicates more heat release and a more stable product. There exist two types of adsorption, if the value of E_{ads} is between -30 to -10 kJ mol⁻¹, the reaction is classified as physical adsorption. Else if the value is between -960 to -50 kJ mol⁻¹, then it belongs to chemical adsorption. Basically, a higher value of E_{ads} corresponds to a stronger adsorption [32].

3. Results And Discussion

3.1. Characterization of materials

N_2 adsorption/desorption isotherm analyzer at liquid nitrogen temperature (77 K) was used to determine the surface area, pore volume, and pore size of SB. The optimal activation ratio of carbonized sludge over $ZnCl_2$ was found to be 1:1. The surface area, pore volume and pore size of the SB-50% $ZnCl_2$ were estimated to be $525 \text{ m}^2 \text{ g}^{-1}$, $0.35 \text{ cm}^3 \text{ g}^{-1}$ and 8.71 nm, respectively. The isotherms belonged to Type IV in the definition of International Union of Pure and Applied Chemistry and indicated that N_2 is condensed in the pores at high relative pressures. There was a hysteresis loop of the H2 style since the pores had a narrow inlet and wide hole, as shown in Fig. 1. The surface area and pore volume in this study higher than Rahman et al. [33] result ($375.32 \text{ m}^2 \text{ g}^{-1}$ and $0.239 \text{ cm}^3 \text{ g}^{-1}$) and Mahmood et al. [34] result ($167 \text{ m}^2 \text{ g}^{-1}$ and $0.16 \text{ cm}^3 \text{ g}^{-1}$).

The functional groups are very important characteristics of the SB, because they determine the surface properties of the SB and their quality. It can provide basic spectra of SB, especially for the determination of types and intensities of their surface functional groups. The changes in the functional groups of different Fe content and appropriate amount of DETA modified on SB were analyzed by FTIR spectroscopy, as shown in Fig. 2. The peak at 3400 cm^{-1} of 8%Fe-SB-DETA is significantly stronger than the peak of other materials. The -OH and N-H stretching vibration band are characteristic peaks of the amine group at about 3400 cm^{-1} [35]. The appearance of peaks at 2930 and 2849 cm^{-1} in the spectrum were attributed to C-H stretching vibration in -CH and $-CH_2$ [35]. The band at 1620 cm^{-1} can be ascribed to C = C aromatic ring stretching vibration [36]. The band at $1470 - 1430 \text{ cm}^{-1}$ is ascribed to C-H bending vibrations in CH_3 groups [35]. C = O vibrations at $1100 - 1000 \text{ cm}^{-1}$ are produced by the stretching vibration of the oxygen-containing functional group C = O bond [37]. There is a weak vibration band between $765 - 530 \text{ cm}^{-1}$, which is judged as an aromatic structure. Due to the large amount of organic matter in the sludge, the chemical structure is composed of a large number of different atoms.

The aim of the XRD studies is to determine the species of SB, SB-DETA and 8%Fe-SB-DETA compounds deposited onto the biochar surface, as show in Fig. 3. The XRD pattern of biochar exhibited one broad diffraction peak corresponding to the diffraction of carbon. A peak at $2\theta = 25^\circ$ was observed for the SB, which was attributed to the carbon in SB. Compared with that of SB, SB-DETA and 8%Fe-SB-DETA, Fe-O typical peak was observed for 8%Fe-SB-DETA at $2\theta = 36^\circ$ and 57° , respectively, shown in Fig. 3 (c).

During the present studies, our aim was to look into the difference in the interaction oxidation/reduction mechanism of metal ions on SB using ECT method. Cyclic Voltammetry (CV) is used to investigate the effect of surface modification, which could provide useful information about the surface states of SB due to the presence of metal vacancy defects on the surface. Figure 4 shows the CV of 2%Fe-SB-DETA, 4%Fe-SB-DETA, 8%Fe-SB-DETA, 16%Fe-SB-DETA and 32%Fe-SB-DETA electrodes in 6 M KOH solution. The bounded area of the CV curve indicates the real active surface area of the anode and the cathode. 8%Fe-

SB-DETA (0.00062 mA) shows a higher current than the 16%Fe-SB-DETA (0.00047 mA), 32%Fe-SB-DETA (0.00044 mA), 4%Fe-SB-DETA (0.00031 mA) and 2%Fe-SB-DETA (0.00023 mA) at the anode. Additionally, 8%Fe-SB-DETA (-0.0016 mA) shows a higher current than the 16%Fe-SB-DETA (-0.0012 mA), 32%Fe-SB-DETA (-0.0011 mA), 4%Fe-SB-DETA (-0.0007 mA) and 2%Fe-SB-DETA (-0.0005 mA) at the cathode. This is indicating that 8%Fe-SB-DETA has a larger active point and better oxidation reduction reaction.

Figure 5 shows the linear sweep voltammetry curves of the samples deposited at different potentials. The currents of the 8%Fe-SB-DETA (0.0027 mA) are improved after being compared with that of 2%Fe-SB-DETA (0.00007 mA) and 4%Fe-SB-DETA (0.0006 mA), indicating that the hydrogen evolution over potential with 8%Fe-SB-DETA is lower than that with 2%Fe-SB-DETA. As a result, 8%Fe-SB-DETA (0.0027 mA) has the largest currents than that the 16%Fe-SB-DETA (0.0012 mA) and 32%Fe-SB-DETA (0.0011 mA). In addition, 8%Fe-SB-DETA composite interface displays a significant change in current–voltage properties as compared to 2%Fe-SB-DETA. The result shows that the electron transfer rate of 8%Fe-SB-DETA is stronger than other materials, which is beneficial to pollutants adsorption.

The current density is tested more than 300 s and maintaining the applied voltage constant at 1.0 mV. Figure 6 shows the currents density are 0.0045, 0.0050, 0.0084, 0.0063 and 0.0060 mA for 2%Fe-SB-DETA, 4%Fe-SB-DETA, 8%Fe-SB-DETA, 16%Fe-SB-DETA and 32%Fe-SB-DETA, respectively. The current of 8%Fe-SB-DETA is 1.9 times larger than that of 2%Fe-SB-DETA, indicating that doping with iron could significantly enhance electron mobility by reducing the recombination of electron-hole pairs.

Electrochemical impedance spectroscopy is a technique to measure the internal resistance of working electrode material and determine the circuitry and corresponding resistance between the electrolyte and the electrode, like biochar carbon in this case. A sine wave of 1.0 mV amplitude was applied and the frequency was varied from 10 KHz to 10 MHz in the 6 M KOH aqueous solution. Ionic and electronic interactions cause the overall impedance of the materials. The larger value of the Z'' (ohm) is indicative of higher resistance due to the transfer of charges. The overall resistance consists of electrical resistance, the resistance due to electrolyte, and the resistance for the carbon pore charge transfer as well as the internal resistance of the material. Result shown in Fig. 7, the 2%Fe-SB-DETA produces high the Z'' value is indicative of higher resistance due to the transfer of charges. The smaller Z'' value of 8%Fe-SB-DETA indicates higher charge carrier transfer efficiency. This determines the effective characteristics of materials as adsorption material. 8%Fe-SB-DETA stands out among all five samples as ideal adsorption material and better adsorption capacity.

3.2. As(III) adsorption capacity with Fe-SB-DETA

The effect of Fe loading mass onto SB-DETA is also discussed in this study. Fe ratio varies with specific dose applied by FeCl_3 during the synthesis process. Different FeCl_3 contents, including 2.0, 4.0, 8.0, 16.0 and 32.0 %, were evaluated with 1.5 g L^{-1} of 8%Fe-SB-DETA at 0.5 mg L^{-1} As(III) with 30 min contact time. The As(III) adsorption experiment was controlled pH 3 to obtain optimum operating conditions in this study, because the valence of As(III) was (\pm) neutral at pH between 2 and 8. However, the valence of

As(III) was (-) negative under pH was larger than 9. In addition, the surface of 8%Fe-SB-DETA was (+) positively charged at pH between 2 and 3. However, the surface of As(III) was (-) negative under pH was larger than 4, as shown in Table 1. Therefore, there is not repulsion between As(III) and 8%Fe-SB-DETA. In this adsorption experiment, first, As(III) is oxidized to form As(V) by 8%Fe-SB-DETA. Afterward, the electrostatic interaction between As(V) and the material. At the same time, As(V) and the amino functional group on the surface of the material will also produce complexation, so that As(V) is adsorbed on the surface of the material.

Table 1
The effect of material surface charge under different pH conditions

pH	2	3	4	5	6	7	8	9	10	11	pH _{zpc}
As(III)	±	±	±	±	±	±	±	-	-	-	
As(V)	±	-	-	-	-	-	-	-	-	-	
8%Fe-SB-DETA	+	+	-	-	-	-	-	-	-	-	3.87

Result shows the removal efficiency of arsenic significantly increases from 30–90% with increasing Fe content from 2.0 to 16.0%. However, the removal efficiency is not changed obviously from 85–90% with increasing Fe content from 8.0 to 16.0%. In contrast, the removal efficiency is decreased from 90–66% with increasing Fe content from 16.0 to 32.0%. In this study, it shows that the Fe impregnated on SB-DETA significantly can enhance the adsorption capacity for arsenic. The higher Fe content does not increase removal efficiency too much when Fe is doped on SB-DETA, maybe the pore of 8%Fe-SB-DETA is blocked. The adsorption capacity of 8%Fe-SB-DETA was calculated as 1.12, 2.23, 3.87, 4.24 and 2.83 mg g⁻¹ with Fe content of 2.0, 4.0, 8.0, 16.0 and 32.0 %, respectively, as shown in Fig. 8.

3.3. Mass balance experiment

Mass balance experiment was conducted to understand the mass before and after arsenic adsorption in the adsorption experiment, as shown in Fig. 9. The adsorption of As was studied with 20 mg L⁻¹ As(III) solution with using 43 g L⁻¹ of 8%Fe-SB-DETA material at pH 3 for 30 min contact time. The remaining concentrations and mass of As(III) and As(V) in 0.2 L solution after adsorption are 1.2 ppm and 0.24 mg; 2.3 ppm and 0.46 mg, respectively. In this specific adsorption, As(III) is oxidized to form As(V) by 8%Fe-SB-DETA. This result has been proved by XPS analysis results that Fe³⁺ reduced to Fe²⁺ after As(III) adsorption. Afterward, the iron oxyhydroxides particles located on the SB-DETA surface are capable of replacing the -OH ligand of As(V) molecules, forming mono or bi-dentate complexes allowing them to be attached to the surface. In addition, the 8%Fe-SB-DETA powder was subjected to a dissolution experiment, and the test results showed that the dissolution concentrations and mass of As(III) and As(V) were 6.8 ppm and 1.36 mg; 9.4 ppm and 1.88 mg, respectively. Result show the total dissolved concentration after arsenic adsorption is 3.94 mg. The concentration of arsenic is lost 0.06 mg, which is

equivalent to $1.5 \pm 0.2\%$. This is caused by the loss of 8%Fe-SB-DETA powder during the dissolution test and filtration process.

3.4. The adsorption configurations of arsenic on Fe-SB-DETA

In order to understand the adsorption mechanism of amine functional group and metal functional group complexes for arsenic adsorbed on the surface of SB and Fe-SB-DETA. Therefore, this study was used DFT to verify the arsenic adsorption mechanisms by SB and Fe-SB-DETA composite material. In this research, single layer structure is used to simulate carbon surface models of SB, as shown in Fig. 10 (a). Figure 10 (b) shown that the arsenic was adsorbed onto SB surface with E_{ads} values of $-27.3 \text{ kJ mol}^{-1}$, indicating a physical adsorption between arsenic and SB surface. This result has proved electrostatic between the positively charged surface of the SB and the anionic arsenic. The results for the adsorption of arsenic on the Fe-SB-DETA surface display all the obtained conformations in Fig. 10 (c-d) and Table 2. It also shows that the bond type, bond distance and adsorption energies. Adsorption configurations were considered in Fig. 10 (c-d) order to achieve the most stable arsenic adsorption configuration. The more monodent conformations have been identified, where the interaction of dopant O with the unprotonated O atom belonging to an As-O bond is formed. The bond distances of N-O and Fe-O are 1.84 and 1.42 Å, respectively, which are shorter for the compounds in compliance with the increased adsorption energies (-93.5 and $-246.3 \text{ kJ mol}^{-1}$), indicating a strong chemical adsorption between arsenic and Fe-SB-DETA surface.

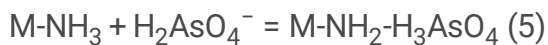
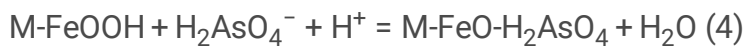
Table 2
Adsorption energies of arsenic adsorbed onto Fe-SB-DETA

Pollutant	Bond	Bond distances (Å)	E_{ads} (KJ mol ⁻¹)
As(III)	C-O (b)	3.52	-27.3
	N-O (c)	1.84	-93.5
	Fe-O (d)	1.42	-246.3

3.5. Mechanism discussion of arsenic adsorption on 8%Fe-SB-DETA

The mechanism for the adsorption of arsenic by 8%Fe-SB-DETA material has been proposed with the results obtained from the characteristics analysis, experimental data and kinetic adsorption. The reaction mechanism is divided into four pathways, as presented in Fig. 11. In the first pathway, first, As(III) is oxidized to form As (V) by 8%Fe-SB-DETA at pH 3, as shown in the formula (3). Afterward, the iron oxyhydroxides particles located on the 8%Fe-SB-DETA surface are capable of replacing the -OH ligand of As(V) molecules, forming mono or bi-dentate complexes allowing them to be attached to the surface [38–40], as shown in the formula (4). The second pathway is the interaction of amino functional groups on

the surface of 8%Fe-SB-DETA with the As(V) molecule produces a complexation interaction, causing As(V) to be adsorbed on the surface of the material, as shown in the formula (5). In the third pathway, the attachment of As(V) ions onto the 8%Fe-SB-DETA via electrostatic interactions, the surface of the material is positively charged and the As(V) ion is negative charged produces electrostatic adsorption under acidic conditions. In this specific adsorption, the coordination only occurs in charged molecules that were previously attracted to the surface of the 8%Fe-SB-DETA, or in those molecules that have energy enough to counteract the electrostatic repulsion with the 8%Fe-SB-DETA surface. Therefore, in 8%Fe-SB-DETA with a negative surface charge, electrostatic repulsion between the surface and As(V) anions occurs. If these ionic molecules have difficulties in overcoming these electrostatic forces they cannot interact to a higher extent with iron particles and hence adsorption occurs to a lesser extent [38]. The fourth pathway is the attachment of As(III) and As(V) ions into the pore of 8%Fe-SB-DETA material via physical adsorption, which may be attributed to Van der Waals forces.



In order to understand whether As(III) is oxidized to As(V), this study uses XPS to detect the material before and after adsorption. The valence state and relative content of As(III) after adsorption was studied with 1.5 g L^{-1} of SB-DETA and 8%Fe-SB-DETA, 0.5 mg L^{-1} As(III) solution, pH 3 and 30 min contact time. XPS peak differentiation-imitating analysis of the As3d spectrum was conducted. The core level spectrum of As3d of the SB-DETA sample reveals the binding energy peaks at 44.3 eV and 45.5 eV corresponding to As(III) and As(V) core levels, respectively. The percentages of As^{3+} (79.15%) and As^{5+} (20.85%) relative to the total Fe were calculated, mainly As^{3+} valence state, as shown in Fig. 12 (a). Figure 12 (b) can be seen that the relative content of As^{3+} after adsorption on the surface of 8%Fe-SB-DETA was reduced to 39.65%; meanwhile, that of As^{5+} increased to 60.35%.

To determine the valence state and relative content of Fe the reaction, XPS peak differentiation-imitating analysis of the Fe2p spectrum was conducted, as shown in Fig. 12 (c, d). The core level spectrum of Fe2p of the 8%Fe-SB-DETA sample reveals the binding energy peaks at 714.5 eV and 728.1 eV corresponding to Fe2p3/2 and Fe2p1/2 core levels, respectively. The photoelectron peaks observed at 714.3 eV and 717.8 eV corresponded to the binding energies of Fe2p3/2, which suggested that the SB-DETA was covered by a layer of iron oxides/hydroxides of iron, such as FeO, Fe_3O_4 and $\text{Fe}(\text{OH})_3$. The percentages of Fe^{3+} and Fe^{2+} relative to the total Fe were calculated. By comparing Fig. 12 (c) and (d), it can be seen that the relative content of Fe^{3+} after the reaction was reduced from 58.28–21.88%; meanwhile, that of Fe^{2+} increased from 41.72–78.12%. This result is consistent with the mass balance experiment, Fe^{3+} (21.88%) are reduced to Fe^{2+} (78.12%) and As^{3+} (39.65%) are oxidized to As^{5+} (60.35%).

In order to understand whether there is complex adsorption between 8%Fe-SB-DETA and arsenic after modification. The functional group changes of 8%Fe-SB-DETA before and after the adsorption of arsenic under different initial concentrations, 1.5 mg L⁻¹ dosage at pH 3 and 30 min, are shown in Fig. 13. The intensity of the characteristic peaks at 3400 cm⁻¹ and 1040 cm⁻¹ was significantly reduced when increased of the arsenic concentration. This result proved the C-NH₃ function group on the surface of 8%Fe-SB-DETA has generated complexation with the arsenic.

4. Conclusions

The results clearly demonstrate the feasibility of using urban sludge as a carbon source to produce biochar. Loading amine and iron on sludge biochar greatly improved its As(III) adsorption capacity. ECT result is indicating that 8%Fe-SB-DETA has a larger active point and better oxidation reduction reaction. Therefore, the highest As(III) removal efficiency is 90% and adsorption capacity is 4.24 mg g⁻¹. Simultaneously, DFT model result is the same as the result of As(III) adsorption performance, because the adsorption energy of Fe-SB-DETA is greater than SB material. The reaction mechanism is divided into four pathways, including oxidation reduction, complexation, electrostatic adsorption and pore adsorption.

Declarations

Availability of data and materials

All data generated or analyzed during this study are examined by our group and certified for several times.

Competing interests

The authors declare they have no competing interests.

Funding

Not applicable

Authors' contributions

Chih-Kuei Chen provided real test data, Thuy-Trang Le supported the test data, Cong-Chinh Duong and Cong-Nguyen Nguyen wrote the paper, Duc-Toan Truong analyzed the test data, and Nhat-Thien Nguyen organized the researched full structure. All authors read and approved the final manuscript.

Acknowledgements

The authors acknowledge financial supports from the Taiwan's Ministry of Science and Technology (MOST 107-2622-E-197-001 -CC3). First author acknowledges the Department of Environmental Engineering, National I-Lan University, Taiwan to support his research at the university.

References

1. Yang R, Su Y, Aubrecht KB, Wang X, Ma H, Grubbs RB, et al. Thiol-functionalized chitin nanofibers for As (III) adsorption. *Polymer*. 2015;60:9–17.
2. Aposhian HV, Maiorino RM, Dart RC, Perry DF. Urinary excretion of meso-2, 3-dimercaptosuccinic acid in human subjects. *Clin. Pharmacol. Ther.* 1989;45:520–526.
3. Mandal S, Sahu MK, Patel RK. Adsorption studies of arsenic (III) removal from water by zirconium polyacrylamide hybrid material (ZrPACM-43). *Water Resour. Ind.* 2013;4:51–67.
4. Choong TSY, Chuah TG, Robiah Y, Koay FLG, Azni I. Arsenic toxicity, health hazards and removal techniques from water: An overview. *Desalination*. 2007;217:139–166.
5. Mondal P, Majumder CB, Mohanty B. Laboratory based approaches for arsenic remediation from contaminated water: Recent developments. *J. Hazard. Mater.* 2006;137:464–479.
6. Mondal P, Bhowmick S, Chatterjee D, Figoli A, Bruggen BV. Remediation of inorganic arsenic in groundwater for safe water supply: A critical assessment of technological solutions. *Chemosphere*. 2013;92:157–170.
7. Song P, Yang Z, Zeng G, Yang X, Xu H, Wang L, et al. Electrocoagulation treatment of arsenic in wastewaters: A comprehensive review. *Chem. Eng. J.* 2017;317:707–725.
8. Kurniawan TA, Sillanpaa ME, Sillanpaa M. Nano adsorbents for remediation of aquatic environment: Local and practical solutions for global water pollution problems. *Crit. Rev. Env. Sci. Tech.* 2012;42:1233–1295.
9. Ray PZ, Shipley HJ. Inorganic nano-adsorbents for the removal of heavy metals and arsenic: A review. *RSC Adv.* 2015;5:29885–29907.
10. Hao L, Zheng T, Jiang J, Zhang G, Wang P. Removal of As(III) and As(V) from water using iron doped amino functionalized sawdust: Characterization, adsorptive performance and UF membrane separation. *Chem. Eng. J.* 2016;292:163–173.
11. Aacharya S, Gaowa N, Ohashi H, Kawamoto D, Honma T, Okaue Y, et al. Adsorption behavior of arsenic to an isolated ferric ion combined on chelate resin. *Bull. Chem. Soc. Jpn.* 2017;90:1372–1374.
12. Zhou Z, Liu Y, Liu S, Liu H, Zeng G, Tan X, et al. Sorption performance and mechanisms of arsenic(V) removal by magnetic gelatin-modified biochar. *Chem. Eng. J.* 2017;314:223–231.
13. Xiong Y, Tong Q, Shan W, Xing Z, Wang Y, Wen S, et al. Arsenic transformation and adsorption by iron hydroxide/manganese dioxide doped straw activated carbon. *Appl. Surf. Sci.* 2017;416:618–627.
14. Karmacharya MS, Gupta VK, Tyagi I, Agarwal S, Jha VK. Removal of As(III) and As(V) using rubber tire derived activated carbon modified with alumina composite. *J. Mol. Liq.* 2016;216:836–844.
15. Bhowmick S, Chakraborty S, Mondal P, Van Renterghem W, Van den Berghe S, Roman-Ross G, et al. Montmorillonite-supported nanoscale zero-valent iron for removal of arsenic from aqueous solution: Kinetics and mechanism. *Chem. Eng. J.* 2014;243:14–23.

16. Dong H, Guan X, Lo IM. Fate of As(V) treated nano zero-valent iron: Determination of arsenic desorption potential under varying environmental conditions by phosphate extraction. *Water Res.* 2012;46:4071–4080.
17. Xu Z, Li Q, Gao S, Shang JK. As(III) removal by hydrous titanium dioxide prepared from one-step hydrolysis of aqueous TiCl_4 solution. *Water Res.* 2010;44:5713–5721.
18. Feng Q, Zhang Z, Ma Y, He X, Zhao Y, Chai Z. Adsorption and desorption characteristics of arsenic onto ceria nanoparticles. *Nanoscale Res. Lett.* 2012;7:1–8.
19. Reddy K, McDonald K, King H. A novel arsenic removal process for water using cupric oxide nanoparticles. *J. Coll. Inter. Sci.* 2013;397:96–102.
20. Tang W, Li Q, Gao S, Shang JK. Arsenic(III, V) removal from aqueous solution by ultrafine $\alpha\text{-Fe}_2\text{O}_3$ nanoparticles synthesized from solvent thermal method. *J. Hazard. Mater.* 2011;192:131–138.
21. Tang W, Li Q, Li C, Gao S, Shang JK. Ultrafine $\alpha\text{-Fe}_2\text{O}_3$ nanoparticles grown in confinement of in situ self-formed “cage” and their superior adsorption performance on arsenic (III). *J. Nanopart. Res.* 2011;13:2641–2651.
22. Akin I, Arslan G, Tor A, Ersoz M, Cengeloglu Y. Arsenic (V) removal from underground water by magnetic nanoparticles synthesized from waste red mud. *J. Hazard. Mater.* 2012;235–236:62–68.
23. Olyaie E, Banejad H, Afkhami A, Rahmani A, Khodaveisi J. Development of a cost-effective technique to remove the arsenic contamination from aqueous solutions by calcium peroxide nanoparticles. *Sep. Purif. Technol.* 2012;95:10–15.
24. Cui H, Su Y, Li Q, Gao S, Shang JK. Exceptional arsenic (III, V) removal performance of highly porous, nanostructured ZrO_2 spheres for fixed bed reactors and the full-scale system modeling. *Water Res.* 2013;47:6258–6268.
25. La DD, Nguyen TA, Jones LA, Bhosale SV. Graphene Supported Spinel CuFe_2O_4 Composites: Novel Adsorbents for Arsenic Removal in Aqueous Media. *Sensors.* 2017;17:1292.
26. Arcibar-Orozco JA, Josue DB, Rios-Hurtado JC, Rangel-Mendez JR. Influence of iron content, surface area and charge distribution in the arsenic removal by activated carbons. *Chem. Eng. J.* 2014;249:201–209.
27. Gao Z, Li M, Sun Y, Yang W. Effects of oxygen functional complexes on arsenic adsorption over carbonaceous surface. *J. Hazard. Mater.* 2018;360:436–444.
28. Materials Studio DMol³. Software users manual for simulate chemical processes and predict properties of materials both rapidly and accurately application. BIOVIA Company; 2018.
29. Perdew JP, Burke K, Ernzerhof M. Generalized gradient approximation made simple. *Phys. Rev. Lett.* 1996;77:3865–3868.
30. Delley B. Hardness conserving semilocal pseudopotentials. *Phys. Rev. B.* 2002;66:155125.
31. Hu L, Peng Y, Wu F, Peng S, Li J, Liu Z. Tubular activated carbons made from cotton stalk for dynamic adsorption of airborne toluene. *J. Taiwan Inst. Chem. Eng.* 2017;80:399–405.

32. Gao Z, Li M, Sun Y, Yang W. Effects of oxygen functional complexes on arsenic adsorption over carbonaceous surface. *J. Hazard. Mater.* 2018;360:436–444.
33. Rahman HL, Erdem H, Sahin M, Erdem M. Iron-incorporated activated carbon synthesis from biomass mixture for enhanced arsenic adsorption. *Water Air Soil Poll.* 2020;231:1–17.
34. Mahmood T, Aslam M, Naeem A, Siddique T, Din SU. Adsorption of As(III) from aqueous solution onto iron impregnated used tea activated carbon: Equilibrium, kinetic and thermodynamic study. *J. Chil. Chem. Soc.* 2018;63:3855–3866
35. Ma Y, Liu WJ, Zhang N, Li YS, Jiang H, Sheng GP. Polyethylenimine modified biochar adsorbent for hexavalent chromium removal from the aqueous solution. *Bioresour. Technol.* 2014;169:403–408.
36. Kilic M, Apaydin-Varol E, Pütün AE. Adsorptive removal of phenol from aqueous solutions on activated carbon prepared from tobacco residues: Equilibrium, kinetics and thermodynamics. *J. Hazard. Mater.* 2011;189:397–403.
37. Jindo K, Mizumoto H, Sawada Y, Sánchez-Monedero M, Sonoki T. Physical and chemical characterizations of biochars derived from different agricultural residues. *Biogeosci. Discuss.* 2014;11:11727–11746.
38. Arcibar-Orozco JA, Josue DB, Rios-Hurtado JC, Rangel-Mendez JR. Influence of iron content, surface area and charge distribution in the arsenic removal by activated carbons. *Chem. Eng. J.* 2014;249:201–209.
39. Jain A, Raven KP, Loeppert RH. Arsenite and arsenate adsorption on ferrihydrite: Surface charge reduction and net OH- Release stoichiometry. *Environ. Sci. Technol.* 1999;33:1179–1184.
40. Sherman DM, Randall SR. Surface complexation of arsenic(V) to iron(III) (hydr)oxides: structural mechanism from ab initio molecular geometries and EXAFS spectroscopy. *Geochim. Cosmochim. Acta*, 2003;67:4223–4230.

Figures

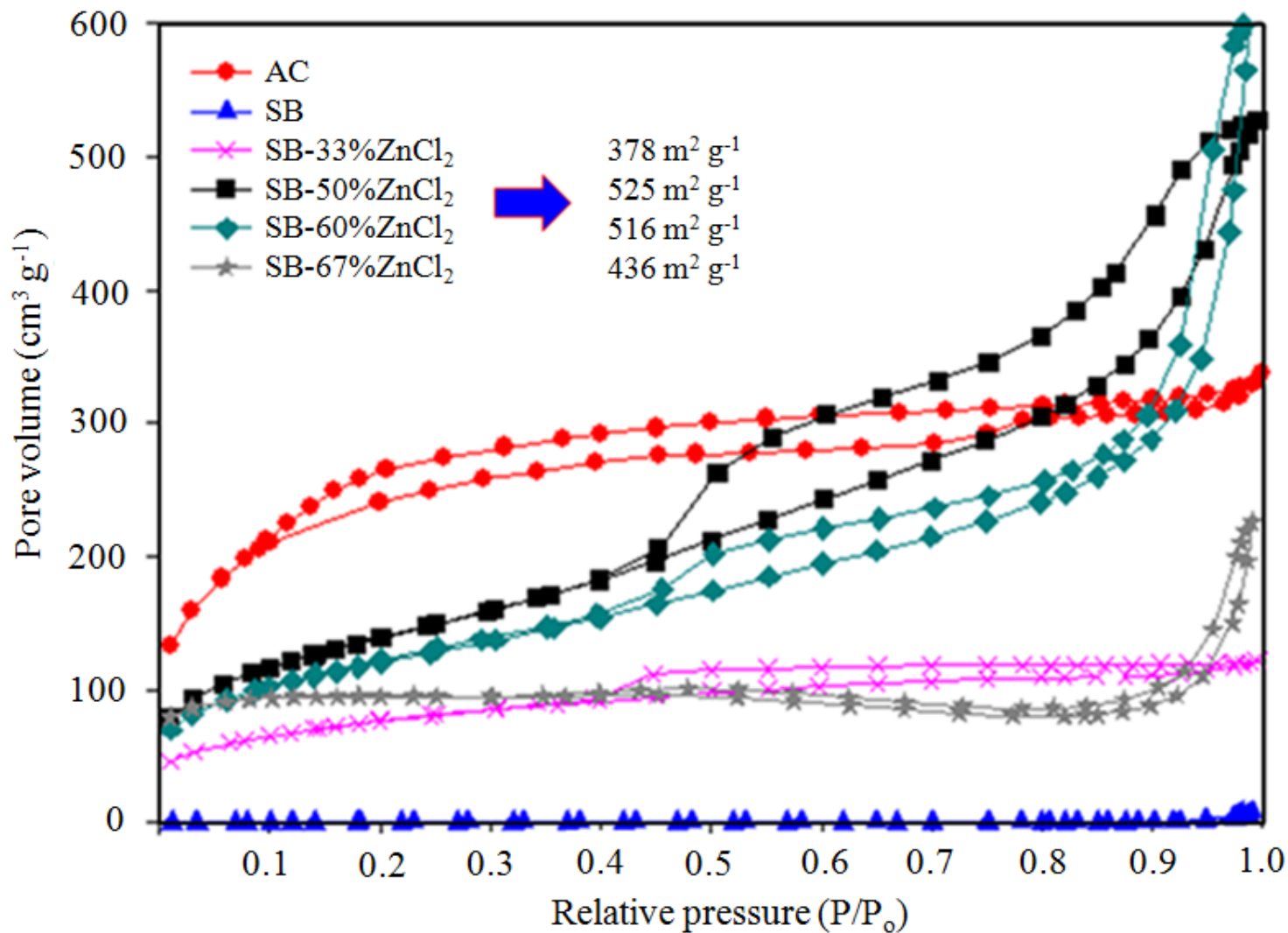


Figure 1

The N₂ adsorption-desorption isotherm of materials

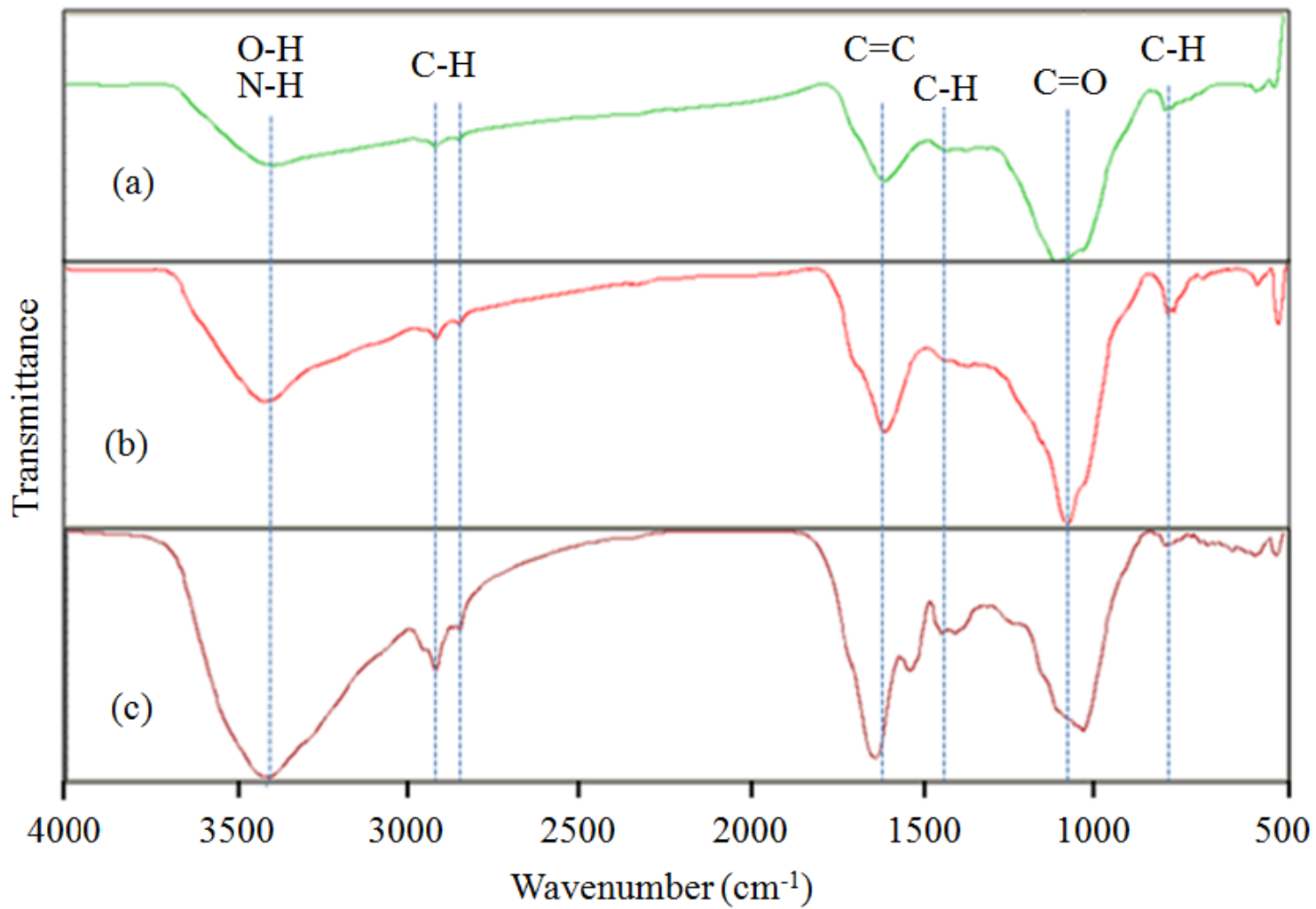


Figure 2

FTIR spectrums of (a) SB, (b) SB-DETA and (c) 8%Fe-SB- DETA

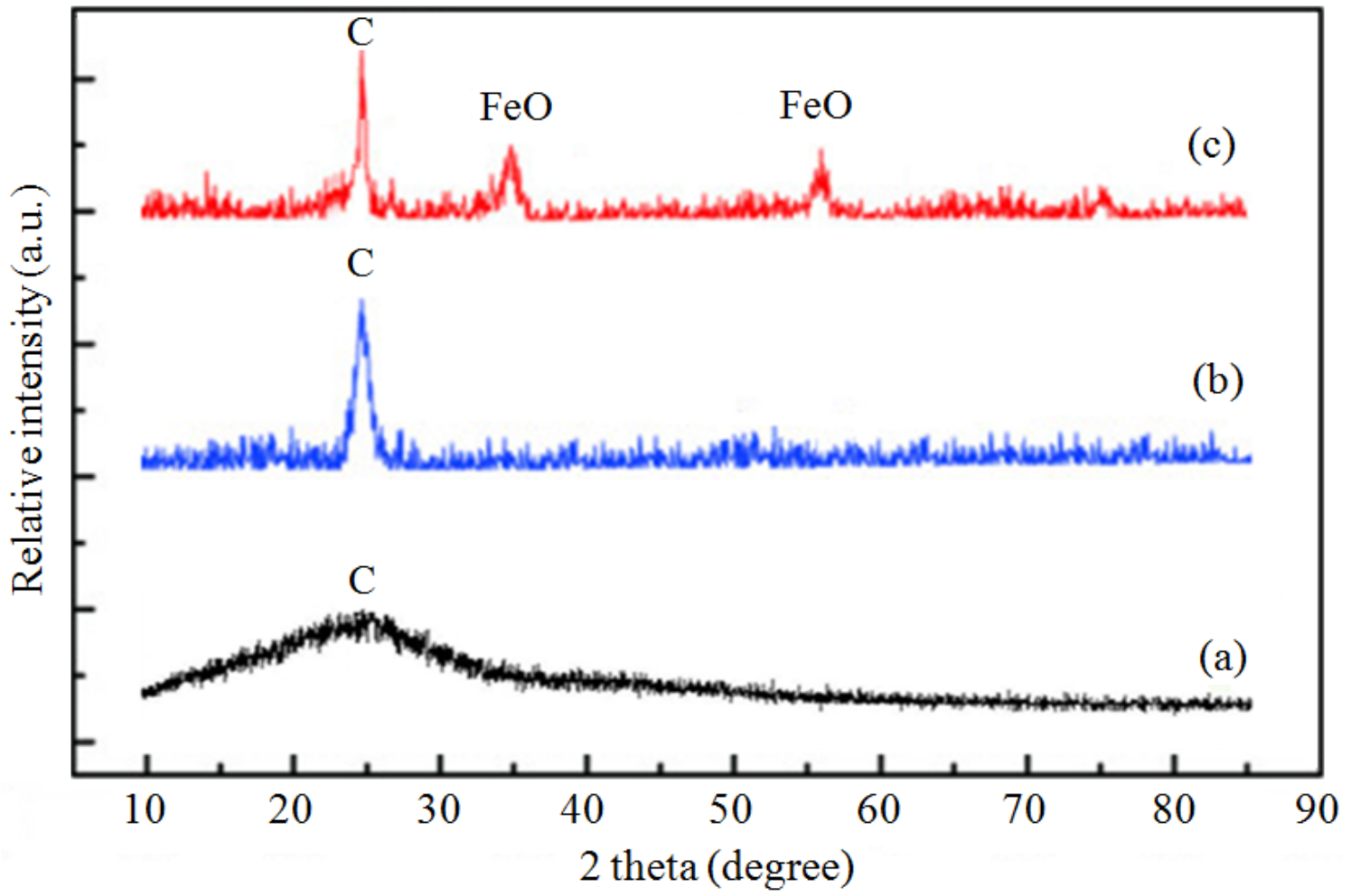


Figure 3

XRD patterns of (a) SB, (b) SB-DETA and (c) 8%Fe-SB-DETA

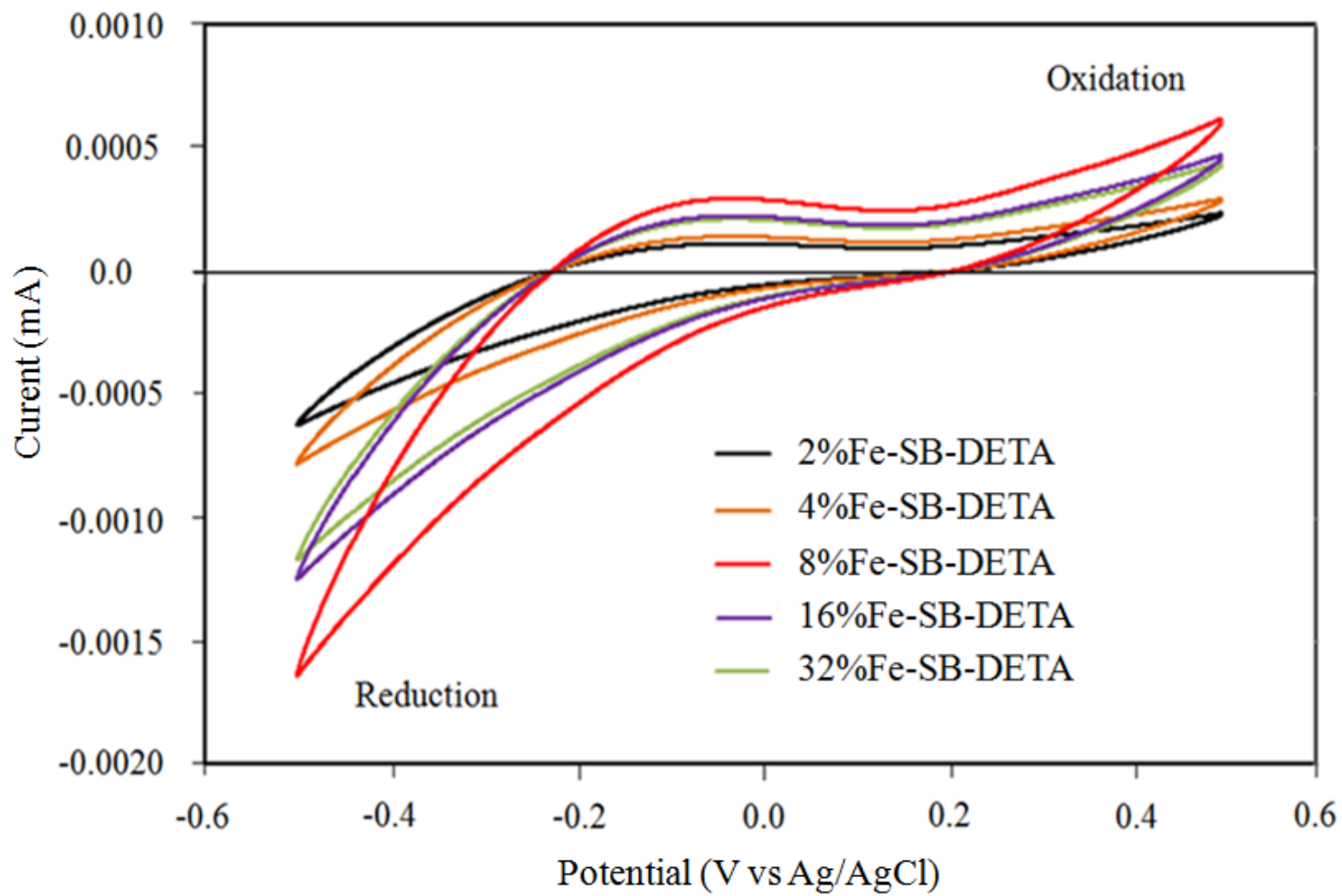


Figure 4

Cyclic voltammograms of biochar electrodes

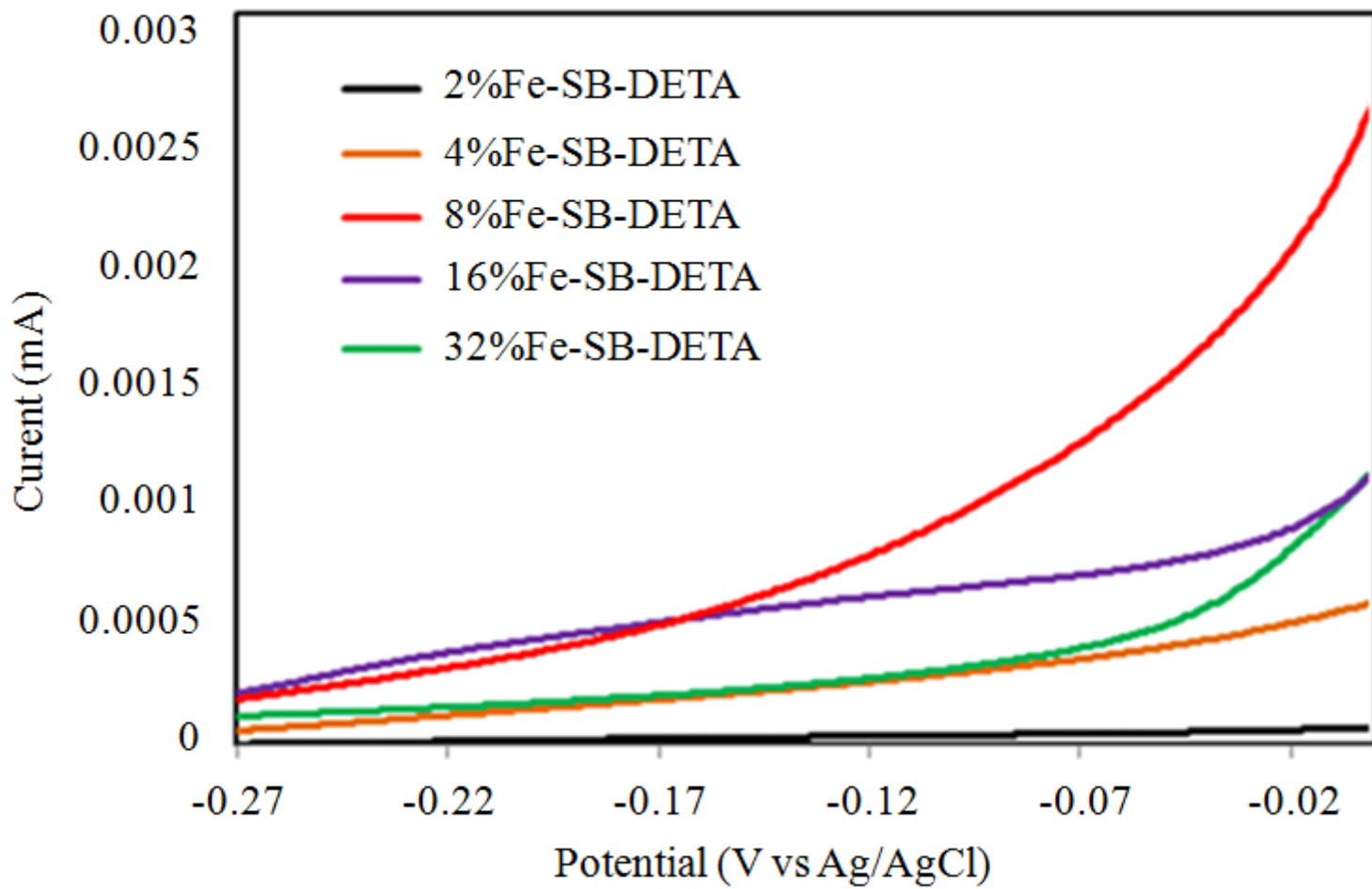


Figure 5

Linear sweep voltammetry curves at different potentials

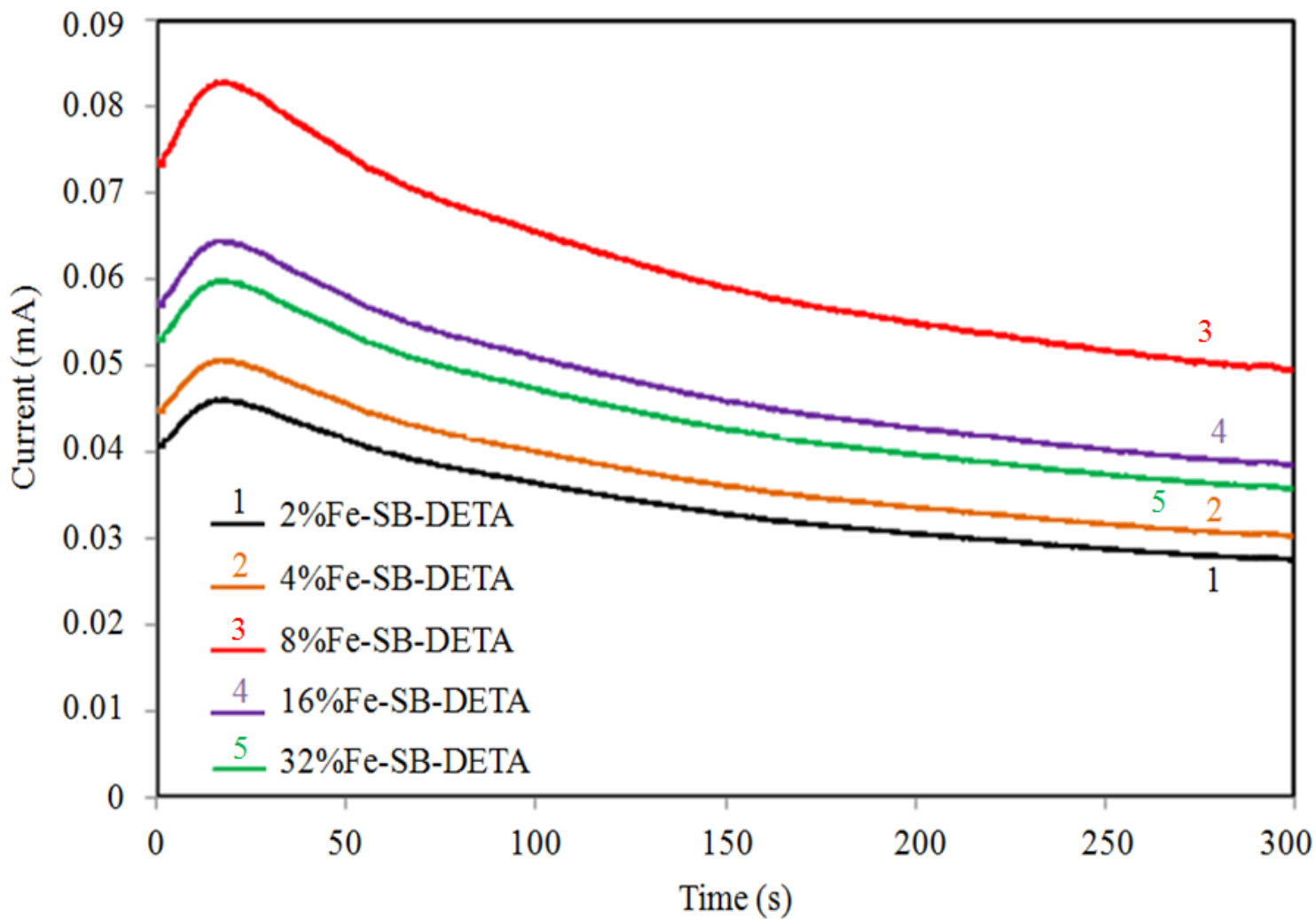


Figure 6

I-t curves of biochar at the bias potential of 1.0 mV

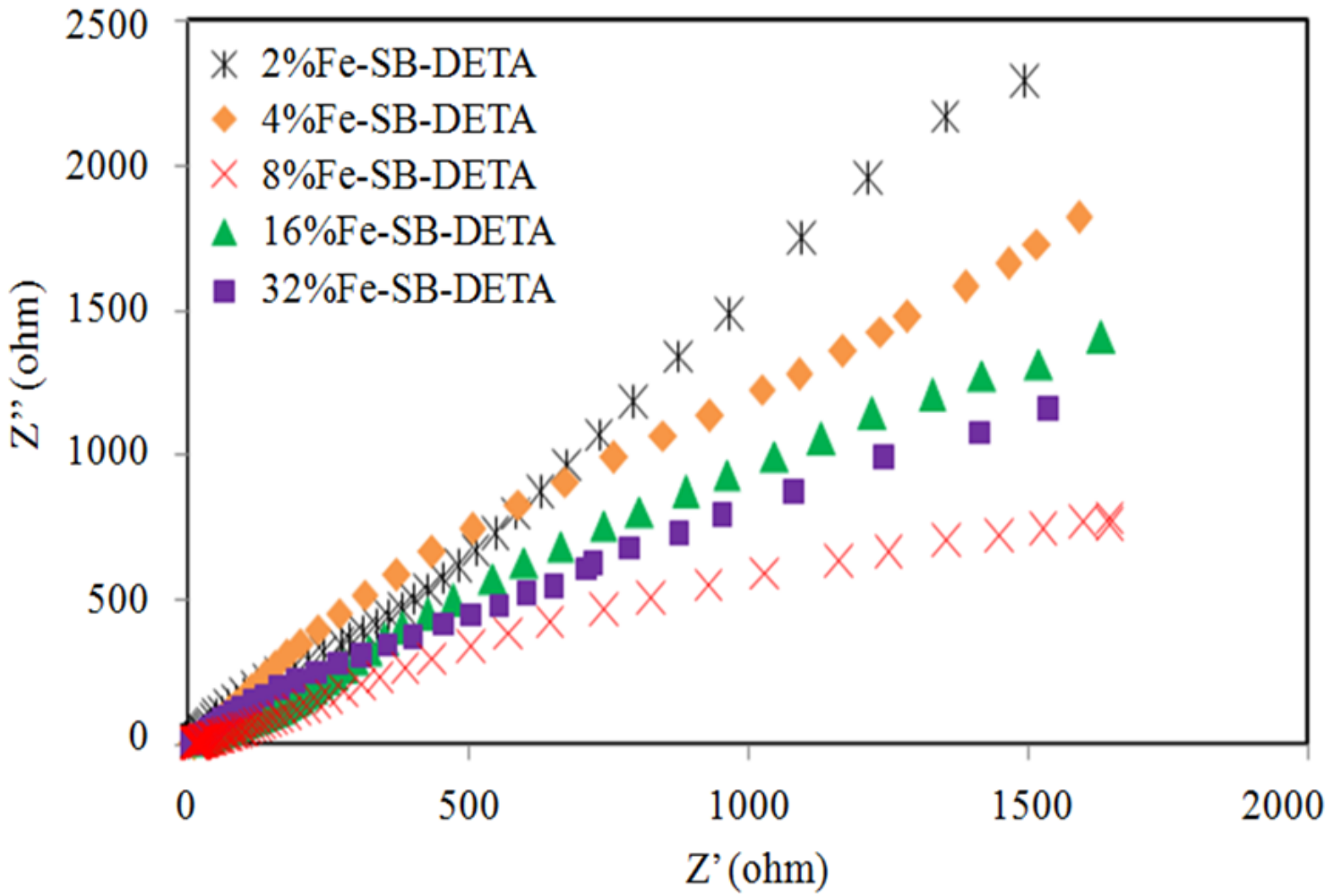


Figure 7

EIS curve for biochar at the bias potential of 1.0 mV

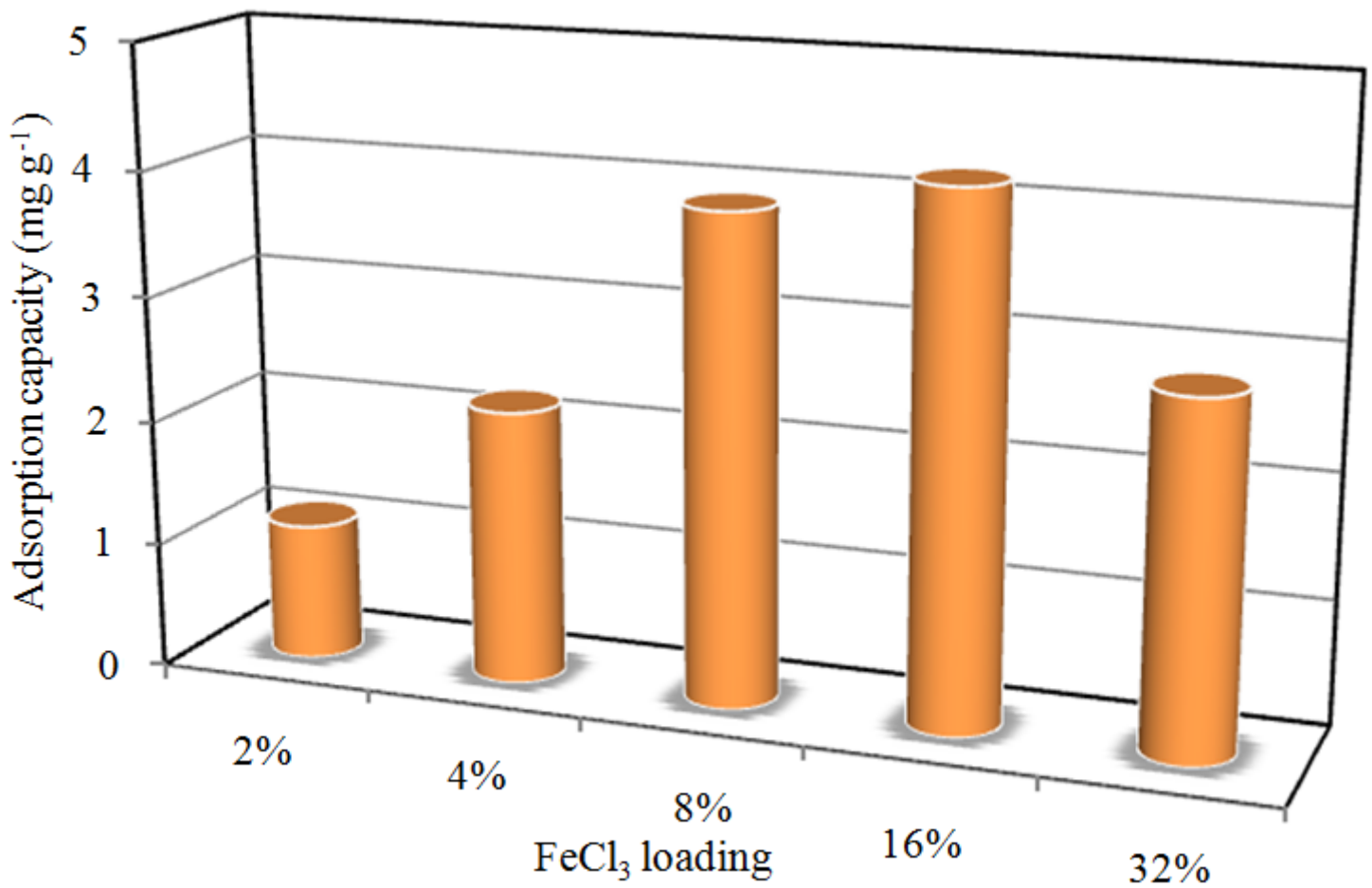


Figure 8

The effect of Fe loading content on the adsorption efficiency

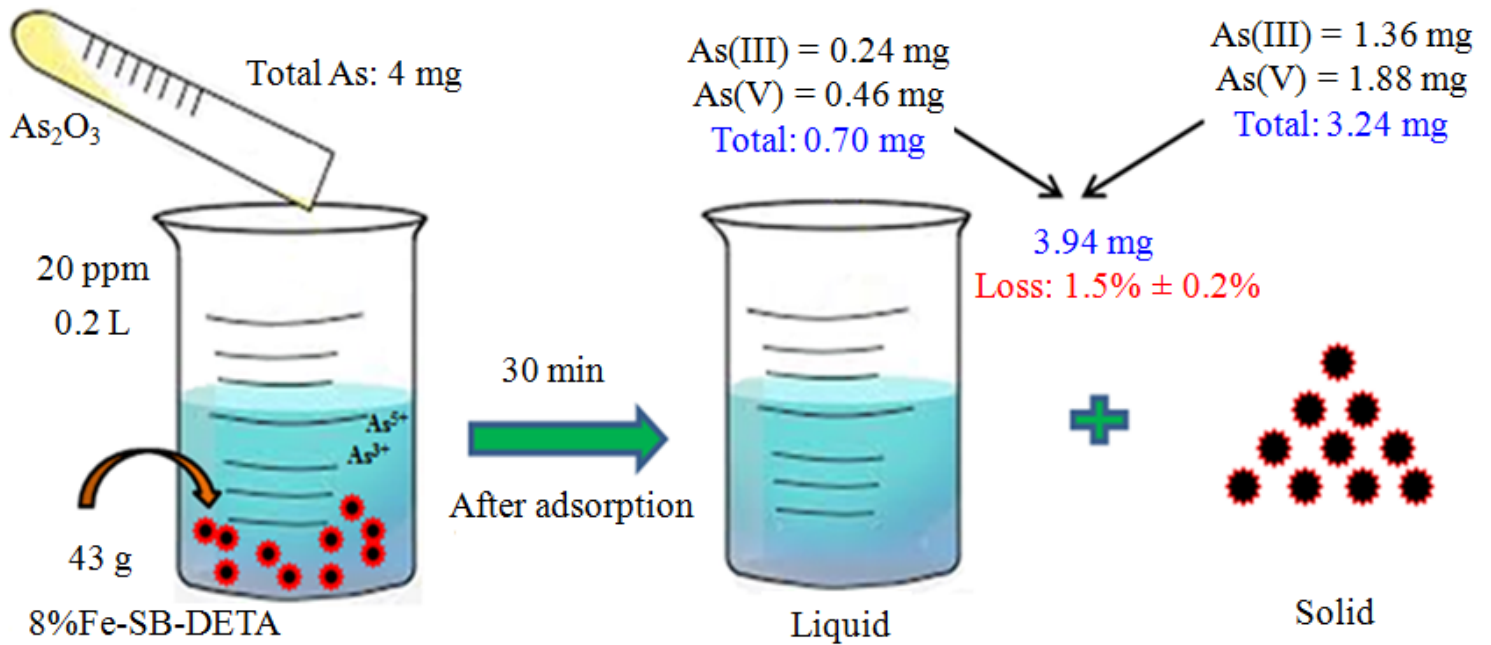


Figure 9

Schematic diagram of mass balance experiment

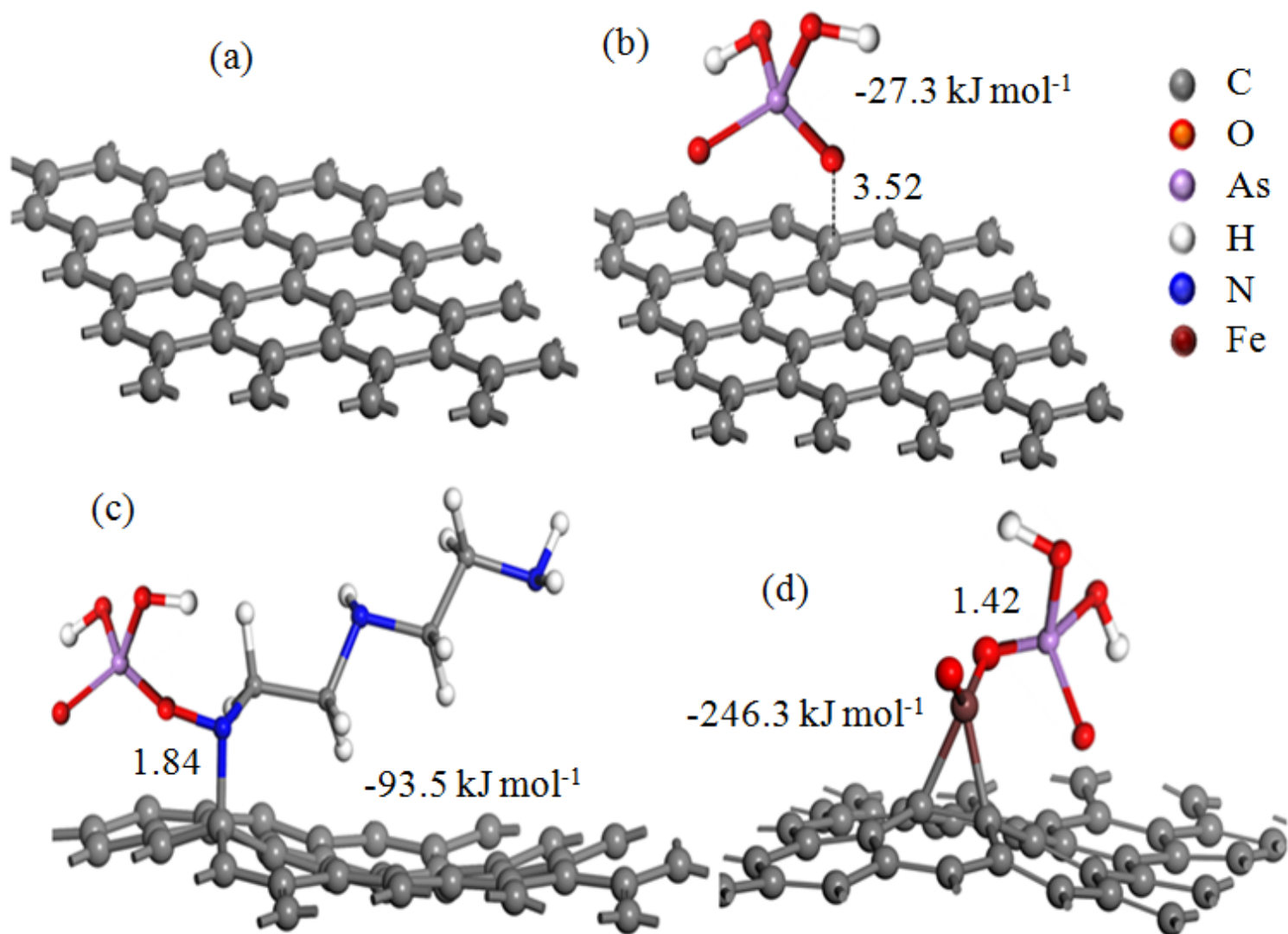


Figure 10

The adsorption configurations of arsenic on Fe-SB-DETA

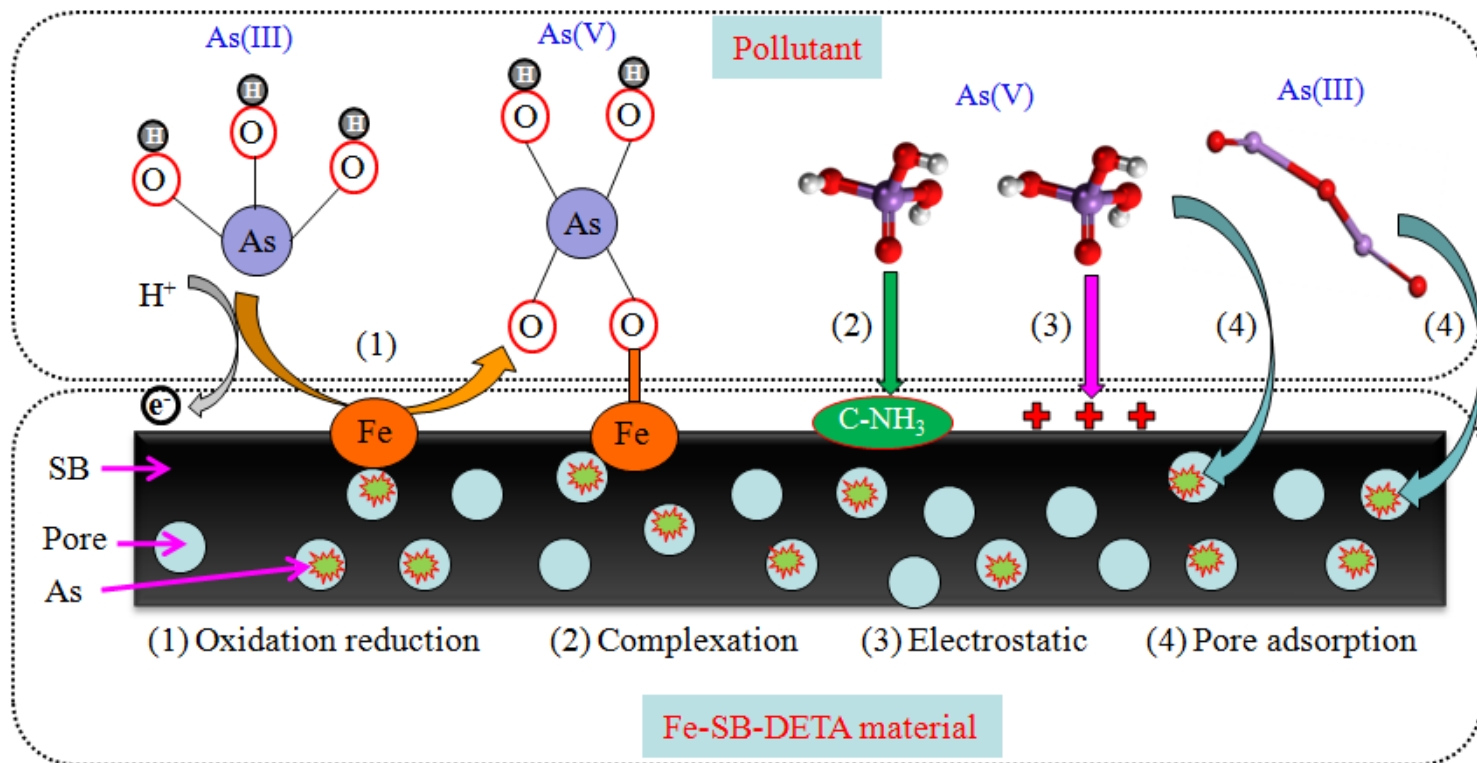


Figure 11

The mechanism of arsenic adsorption on 8%Fe-SB-DETA

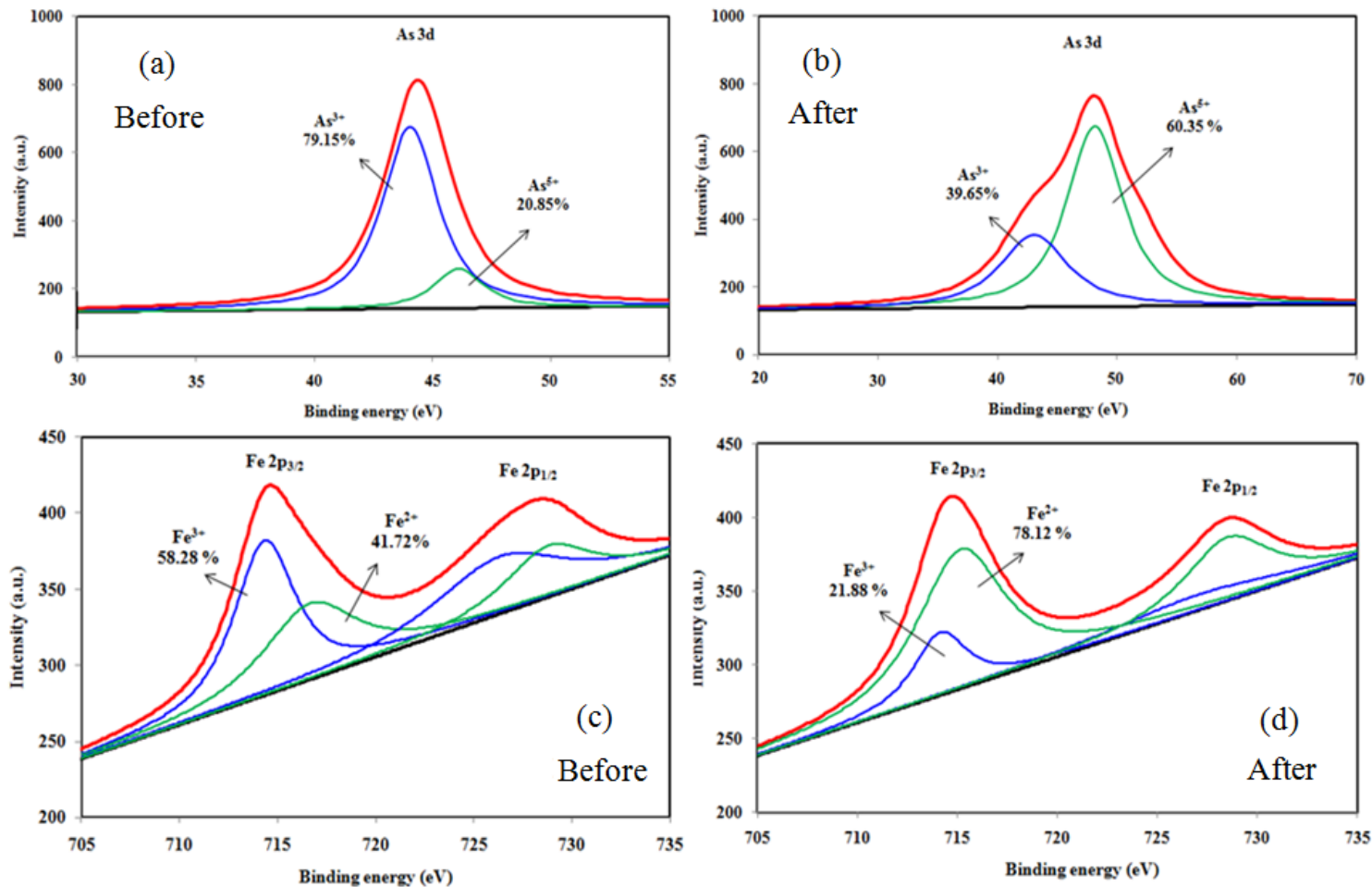


Figure 12

XPS of the As3d and Fe2p state of arsenic before and after adsorption present in 8%Fe-SB-DETA

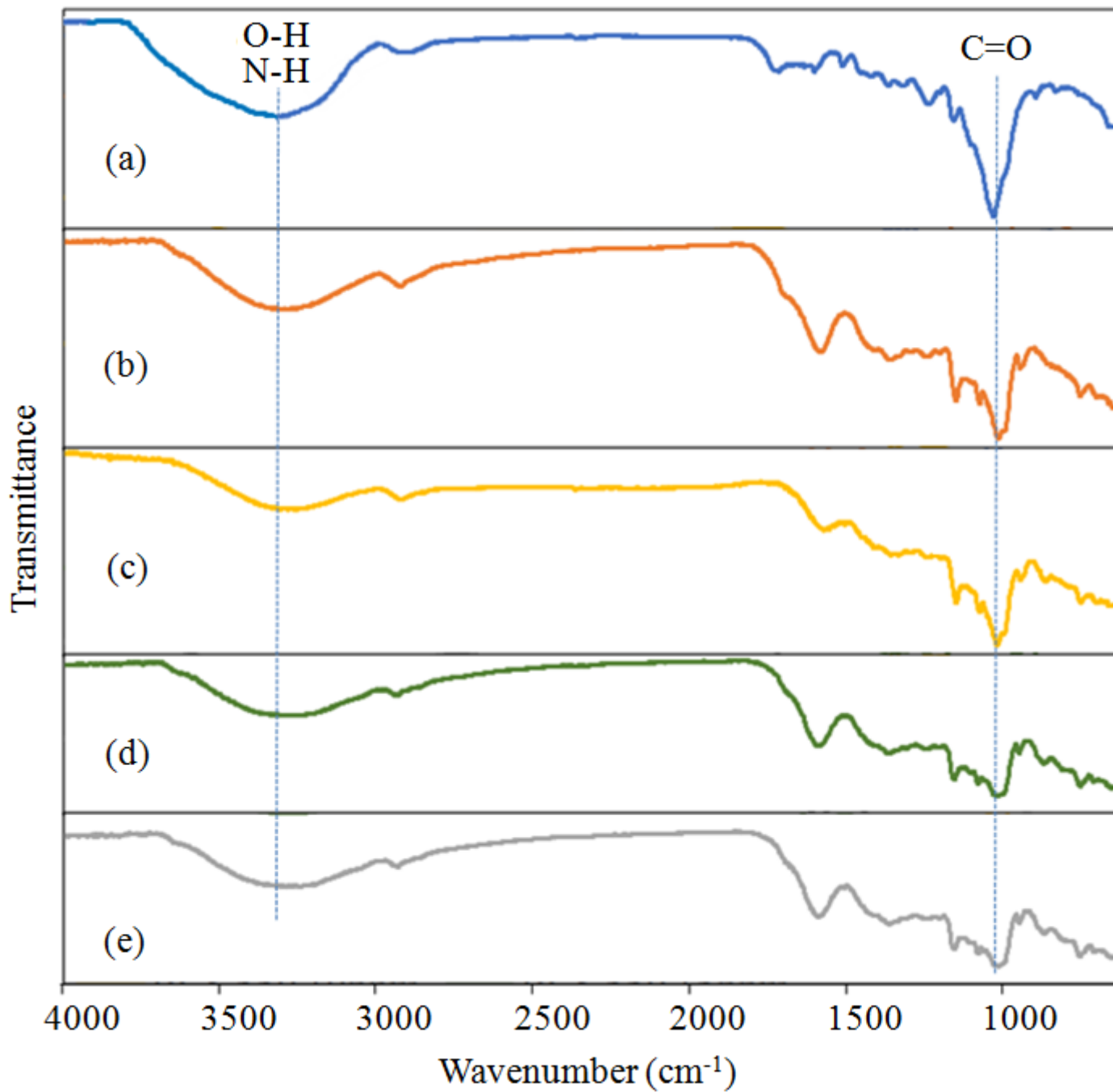


Figure 13

FTIR spectrums of (a) 8%Fe-SB-DETA and after adsorption As(III) with (b) 0.2 ppm, (c) 0.4 ppm, (d) 0.6 ppm and (e) 0.8 ppm